Gyroscope prototype with active magnetic levitation and switched reluctance propulsion

Marius PAKŠTYS*, Renato GALLUZZI**, Luis MIGUEL CASTELLANOS*, Angelo BONFITTO*, Andrea TONOLI* and Nicola AMATI*

* Department of Mechanical and Aerospace Engineering, Politecnico di Torino
Turin, 10129, Italy
E-mail: marius.pakstys@polito.it

** School of Engineering and Sciences, Tecnologico de Monterrey
Mexico City, 14380, Mexico

Abstract

A gyroscope system with a shaftless annular flywheel design supported by means of active magnetic bearings is presented. Elimination of contact friction, as well as a homopolar electromagnet arrangement aims to reduce drag forces that become significant at high speeds. The system is intended for applications where low maintenance is required, and where power consumption is important. Indeed, the gyroscope can be exploited in applications where resultant torque is desired on a perpendicular axis. Functional tests consisting of rotor lift-off, external disturbance imposition, and switched reluctance motor actuation are executed. Results demonstrate the viability of installing active magnetic suspension in gyroscopes. Motor performance improvement is achieved by including a lead activation, and lag deactivation of current phases. Limitations due to magnetic drag are evidenced in the rotor speed profile. Results also indicate operational considerations, such as rotordynamic contributions due to flywheel surface irregularities.

Keywords : Gyroscopic effect, Flywheel, Active magnetic bearings, Functional testing

1. Introduction

The gyroscopic effect is relevant for several applications, including vehicle stabilisation, attitude control, and energy harvesting. Conventional bearings used to support the rotating flywheel are cost-effective, however they introduce significant mechanical losses at high speed. Active magnetic bearings (AMBs) can be used as a substitute, eliminating contact friction. Adequate stiffness can be ensured with proper control strategy design. A previous study presented an AMB controlled reaction flywheel for satellite applications (Hsiao and Hsieh, 2023). In Li et al. (2021), AMBs are exploited for an energy storage system. Another study presented a flywheel battery for vehicle applications (Zhang and Yang, 2024). Most investigations focus on energy storage, and all prototypes rely on permanent magnet force biasing. The present work gives an overview of a gyroscopic system with a shaftless ring shaped rotor, installed with AMBs. Indeed, the unconventional design of the rotor necessitates a particular system topology. Switched reluctance motor (SRM) elements are integrated such that a constant rotational speed can be achieved. The study addresses system description, and functional testing consisting of levitation and motor actuation, verifying the feasibility of using AMBs for gyroscope system applications. The work presents the gyroscope features in a simple layout using a fully active levitation approach. Moreover, electromagnets are arranged in a homopolar configuration, ensuring reduced magnetic drag incident on the rotor.

The remainder of the manuscript is organised as follows. Section 2 presents an overview of the system regarding AMB and SRM electromagnet layout, as well as use of microprocessors, power stages, and sensors. Functional tests including lift-off, application of external perturbation, and SRM performance are discussed in Section 3. Frequency content in recorded signals is evaluated for measurements in conditions of external disturbances. The analysis is repeated for the case of rotation under SRM actuation. Finally, Section 4 concludes the work.

2. System overview

The gyroscope consists of several key features. A ferromagnetic annular reaction flywheel is the levitated component. Its shaftless and diametrically homogeneous configuration means electromagnetic forces are directly imposed on the rotor. This differs from conventionally levitated flywheels where AMBs are positioned about shaft sections with reduced diameters. Table 1 reports a summary of the flywheel characteristics. The rotor is situated in a drum structure, housing also the electromagnets. Note that it is characterised by a non-laminated manufacture.

Table 1 Characteristic parameters of the rotor in the gyroscope prototype

Parameter	Description	Value	Units
R_e	External radius	250	mm
R_i	Internal radius	187.5	mm
h	Rotor thickness	18	mm
m	Rotor mass	13	kg
J	Rotor inertia	0.61	kgm^2

2.1. Electromagnets

The axial (z-axis) direction is outfitted with eight AMBs above and eight below the flywheel in a symmetric configuration. A further six AMBs are installed in the radial (x- and y-axis) orientation. The x-axis relies on four AMBs, whereas the y-axis makes use of two. The controlled degrees of freedom (DOFs) are linear displacements in x-, y-, and z-axes, as well as angular displacements about the x- and y-axes, denoted by ψ and ϑ respectively. Flywheel motion is induced with a SRM using another six dedicated electromagnets, positioned radially. Table 2 indicates the number of turns and peak force of the electromagnets. Nominal air gap is set to 0.6 mm for all actuators. Wire diameters are sized for a peak current density of 8 A/mm^2. Figure 1(a) reports a schematic of the prototype, with its main features. Radial AMBs are not shown, however their design and placement are analogous to SRM electromagnets.

Table 2 Key features of electromagnets installed in gyroscope prototype

Parameter	Description	x-axis	y-axis	z-axis	SRM	Units
N	N. turns	100	100	83	45	–
F_{pk}	Peak force	83	185	1534	-	N

2.2. Sensors and control

Closed-loop position control is implemented with a set of proximity sensors and conditioning circuits that relay position information to microprocessors generating control signals. The axial direction makes use of four proximity sensors, whereas the radial direction exploits two for each axis. Teeth on the inner rotor diameter interact with reflectance sensors to guarantee appropriate activation of the three current phases. Three reflectance sensors are used to measure relative angular position between rotor and SRM electromagnet poles. TI F28379D LaunchPad cards are used in the hardware setup. They are designated as primary or secondary boards. Primary boards provide control commands to secondary boards. For the z-axis, eight microprocessors are installed, one being a primary board. For radial control, one primary board per axis is used, relying on no secondary boards. The SRM relies on one primary board for each of the three current phases. To execute pulse-width modulation commands, TI BOOSTXL DRV8323RS power stages are used. For axial control, 16 are coupled with the microprocessors. In radial control, two power stages are used per axis. The SRM requires two power stages per phase. Figure 1(b) indicates the prototype mounted on a support structure for testing. The support structure allows for free rotation about the x-axis.

Proportional-Integral-Derivative (PID) control is implemented to guarantee nominal air gap. Five position controllers are used to generate control current references for each DOF. Position sensor data is subject to a coordinate transformation. This approach guarantees an averaging of measurements, to avoid exciting certain rotor mode shapes. Indeed, the slender geometry of the rotor necessitates consideration of the impact of its deformation on control stability. The output

coordinates refer to controlled DOFs. Proportional-Integral (PI) controllers are implemented for inner current loops, all featuring a closed-loop bandwidth of 1 kHz.

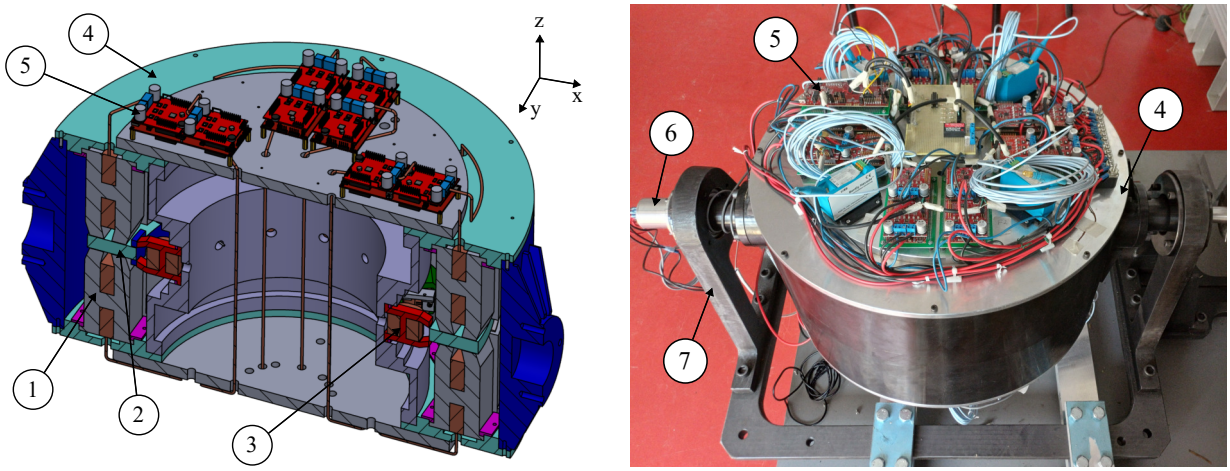

(a) (b)

Fig. 1 Prototype with main features. (a) Schematic indicating key elements. 1. Axial AMB; 2. Reaction flywheeel; 3. SRM electromagnet; 4. Housing structure; Microprocessing hardware. (b) Experimental test setup for gyroscope prototype. 6. Slip ring; 7. Support structure.

3. Functional testing and results

Several tests are performed to verify the performance of the system. Firstly, a lift-off test ensures correct AMB operation. Secondly, external angular disturbances are imposed. Perturbations are applied by the user, however dominant frequency content is nonetheless identified. Finally, SRM performance is evaluated regarding its speed profile. Additionally, lead and lag phase actuation are introduced in SRM actuation to attain higher speeds.

3.1. Lift-off

Regarding lift-off, the time histories of the main DOFs are recorded. MATLAB and Simulink are used to communicate with a central microprocessor via serial bus, as well as to sample data. Figure 2(a) reports the displacements in the z-, x- and y-axes. The control current for each DOF is included. Stable levitation is confirmed after 100 ms, when steady-state conditions are reached for the axial DOF. The settling time for the radial DOFs is shorter due to lower lateral inertia. Note that the current consumption in the axial direction is biased to sustain a portion of the flywheel mass against gravity. Moreover, Fig. 2(b) indicates similar behaviour during lift-off for position and current in the rotational DOFs.

3.2. Disturbances

In a further test, the flywheel is levitated, and angular disturbances are imposed on the drum. The SRM is not engaged. Disturbances are characterised by an application of oscillatory angular displacements of the prototype about the x-axis, facilitated by the support structure. The amplitude of the oscillations is approximately 15 deg. Figure 3(a) identifies the recorded axial displacements in the presence of disturbances. Notably, a larger instantaneous current demand is present due to vibratory compensations. Figure 3(b) indicates radial displacements and control currents.

Figure 4(a) highlights the response of the rotational DOFs. Angular displacement about the x-axis (ψ) presents greatest perturbation. Moreover, the Fast-Fourier Transform (FFT) is applied on the acquired time domain data of angular displacement about the x-axis (ψ), reported in Fig. 4(b). The most dominant harmonic contribution corresponds to approximately 2 Hz. The frequency content reflects a critical condition that may be reached in a specific application environment. The same frequency content is also expected to be present in the y-axis displacement data.

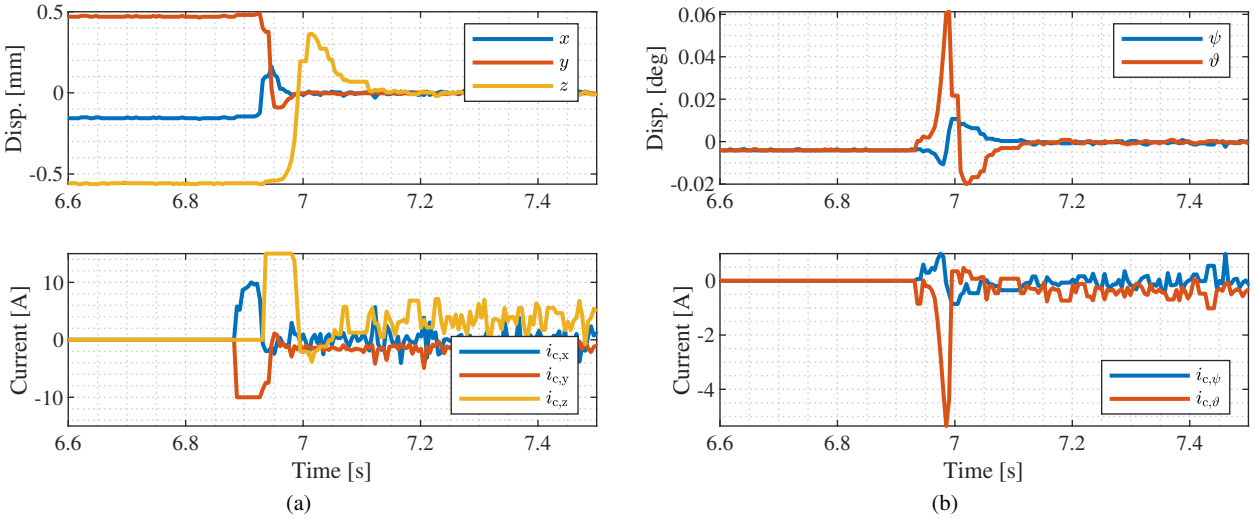

Fig. 2 (a) Axial and radial displacements during rotor lift-off with associated control currents. (b) Angular displacements and associated control currents during rotor lift-off.

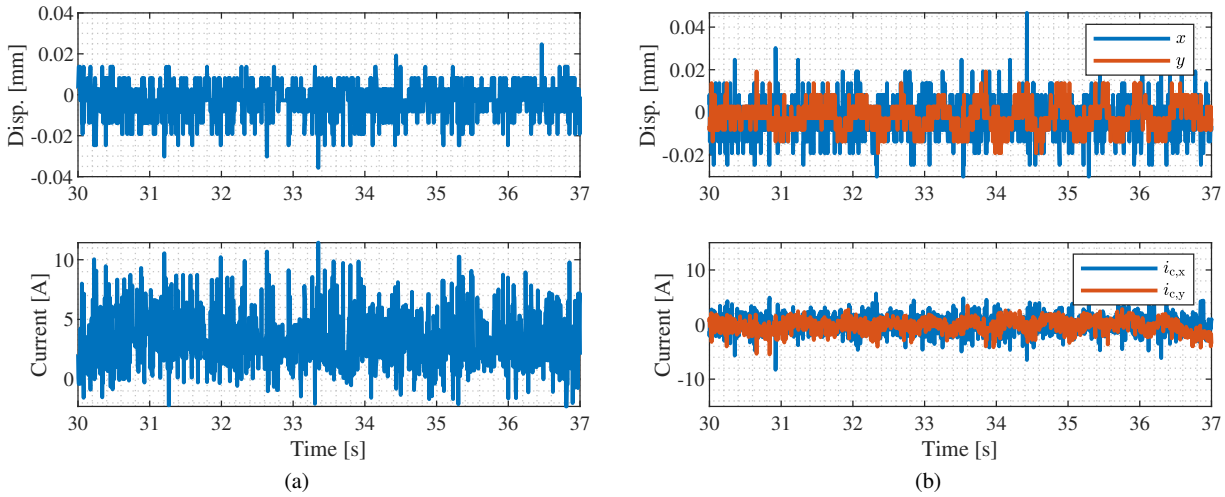

Fig. 3 (a) Axial displacement and associated current under external perturbations. (b) Radial displacements and associated control currents in presence of external disturbances.

3.3. Switched reluctance motor

To test the motor, the rotor is levitated, and the three SRM phases are actuated (setting also the current amplitude), bringing the flywheel to steady-state rotation. Due to reflectance sensor dynamics, SRM control includes a lead activation angle, α, and a lag deactivation angle, β, of each phase (in electrical degrees) such that greater torque is delivered. These values are modified on-line using the MATLAB and Simulink model communicating with microprocessors. Figure 5(a) indicates different operating setpoints tested for the SRM. Greater speed is guaranteed with non-null activation and deactivation. Increasing the current amplitude further increases speed. An operating setpoint of $i_{\text{mot}} = 16$ A, $\alpha = -20$ deg, and $\beta = 30$ deg is chosen to further assess the SRM. Figure 5(b) reports the SRM speed profile with portions attributed to acceleration, steady-state, and deceleration. Note that acceleration and deceleration times differ. Indeed, axial electromagnets are arranged in a homopolar configuration with intermediate spacing. Discontinuities in the magnetic flux density profile in the track generate eddy currents. These are responsible for a magnetic drag torque incident on the rotor. At higher speeds, their effect is more prominent. As speed increases during rotor run-up, resistant torque increases.

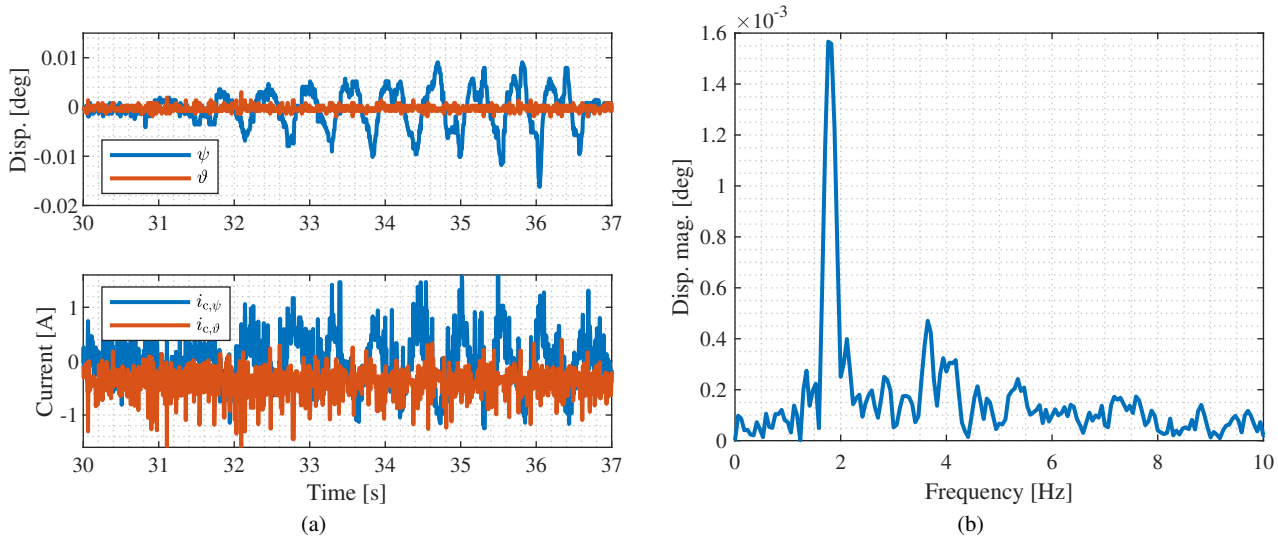

Fig. 4 (a) Angular displacements under external perturbations. (b) FFT for angular displacement about x-axis (ψ).

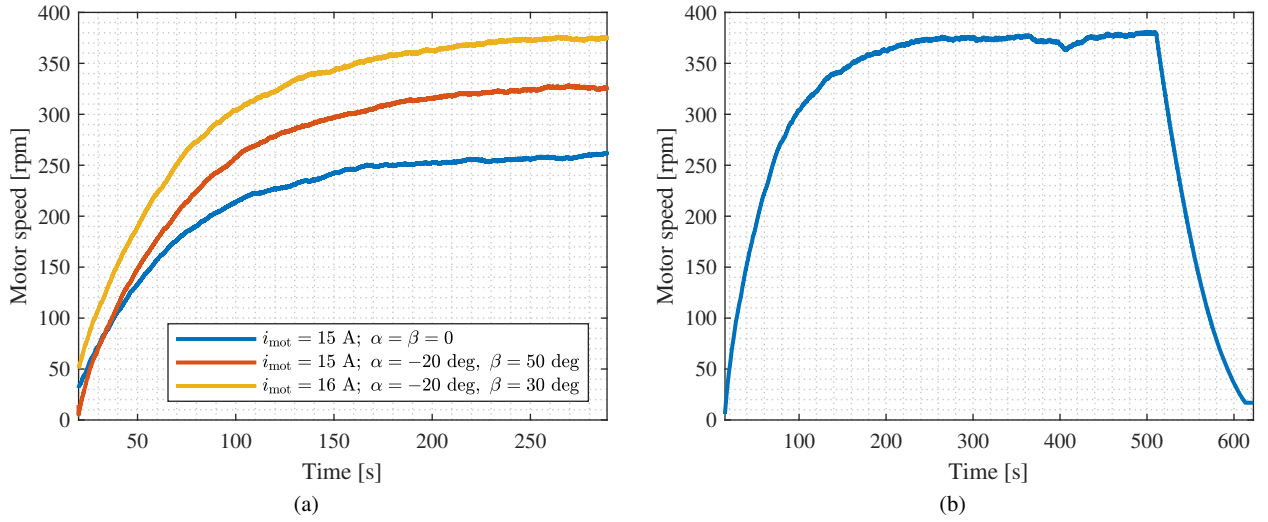

Fig. 5 (a) Motor speed tuning by means of current and phase activation timing variation. (b) Top speed reached during functional testing with $i_{\mathrm{mot}} = 16$ A, $\alpha = -20$ deg, and $\beta = 30$ deg.

An effect from the induced flywheel rotation can be identified in the radial AMBs. Figure 6(a) indicates the recorded signal of displacements in x- and y-axes. Displacement amplitudes increase due to the additional presence of rotordynamic contributions. Figure 6(b) highlights the frequency content of the y-axis displacement signal. Given a rotational speed of $\Omega = 380$ rpm, the frequency of the first harmonic corresponds to $f_1 = 6.3$ Hz, visible in the plot. The FFT also presents contributions at $f_2 = 12.6$ Hz and $f_3 = 18.9$ Hz, corresponding to second and third harmonics respectively. These harmonics emerge due to irregularities on the flywheel surface, and represent dynamic contributions in the overall operation of the system.

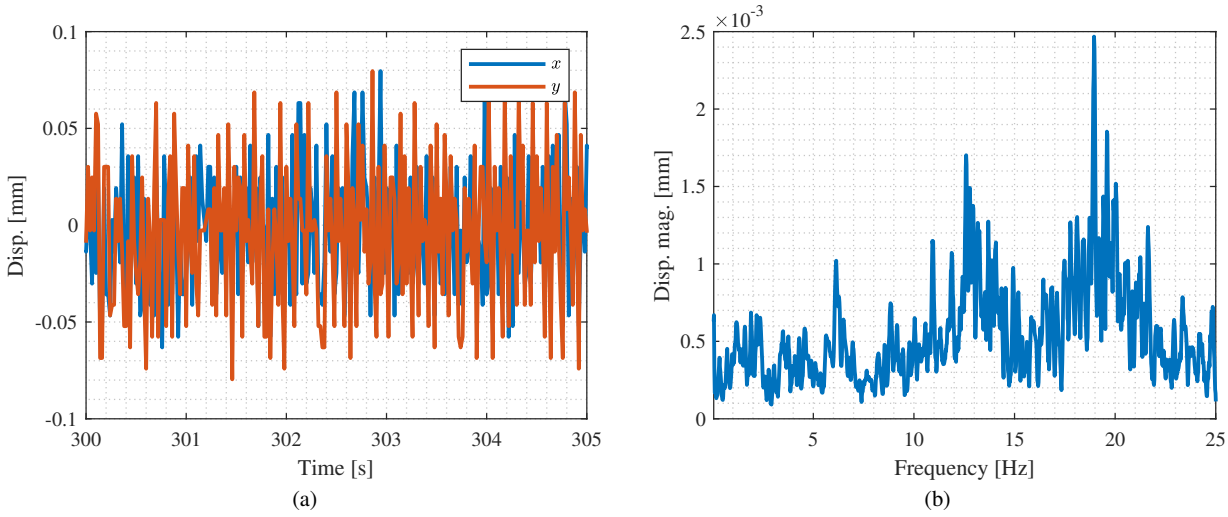

Fig. 6 (a) Radial displacement during motor steady state operation with $i_{\mathrm{mot}} = 16$ A, $\alpha = -20$ deg, and $\beta = 30$ deg. Motor speed at $\Omega = 380$ rpm. (b) FFT of y-axis displacement with motor speed at $\Omega = 380$ rpm.

4. Conclusions

An overview of the main features and their role in an experimental gyroscopic test bench is presented for a magnetically levitated reaction flywheel supported by AMBs. Functional tests pertaining to levitation and SRM actuation are reported and discussed. The results show the designed system can sustain stable levitation of the flywheel during lift-off and in the presence of disturbances featuring a dominant contribution at 2 Hz. The SRM is also studied regarding its speed capability. Indeed, it is clear that a lead activation together with a lag deactivation of phase currents extends the time the rotor teeth are subjected to electromagnetic torque. Increased rotational speed is hence guaranteed. The presented system highlights the feasibility of replacing conventional mechanical bearings with AMBs to reduce mechanical losses in gyroscopic systems. Such systems are suitable for a number of applications where a resultant gyroscopic moment at a desired axis is needed. Examples include attitude control and energy harvesting. Operational considerations from the rotordynamics point of view are shown to be important for overall performance. Magnetic drag in the homopolar electromagnet design is also a key factor for power consumption. Future work involves the introduction of deterministic disturbances via a Power-Take-Off (PTO). The evaluation of losses of the homopolar levitation system using flywheel rundown data is also provisioned in further investigation.

References

D. Hsiao, M. Hsieh, “Design and Implementation of Novel Homopolar Magnetic Bearings Incorporated in Reaction Wheel for Satellite Attitude Control.” IEEE Access, vol. 11, 2023, pp. 66374–81. DOI.org (Crossref), https://doi.org/10.1109/ACCESS.2023.3290308.

X. Li, A. Palazzolo, Z. Wang, “A Combination 5-DOF Active Magnetic Bearing for Energy Storage Flywheels.” IEEE Transactions on Transportation Electrification, vol. 7, no. 4, Dec. 2021, pp. 2344–55. DOI.org (Crossref), https://doi.org/10.1109/TTE.2021.3079402.

W. Zhang, J. Yang, “Multiphysics Fields Analysis and Optimization Design of a Novel Saucer-Shaped Magnetic Suspension Flywheel Battery.” IEEE Transactions on Transportation Electrification, vol. 10, no. 3, Sept. 2024, pp. 5473–83. DOI.org (Crossref), https://doi.org/10.1109/TTE.2023.3318305.